AGU ADVANCING EARTH AND SPACE SCIENCES

Geophysical Research Letters

RESEARCH LETTER
10.1029/2025GL118498

Detection of Submerged Targets Beyond Eyes' Observation Using Satellite Lidar and Multispectral Data

Hao Liu[1], Jian Yang[1], Yue Ma[1,2], Yao Li[3], and Xiao Hua Wang[4]

[1]School of Electronic Information, Wuhan University, Wuhan, China, [2]Wuhan Institute of Quantum Technology, Wuhan, China, [3]School of Geographical Science, Southwest University, Chongqing, China, [4]Sino Australian Research Consortium for Coastal Management, School of Science, University of New South Wales, Canberra, ACT, Australia

Key Points:

- A framework to detect submerged targets is proposed solely on satellite data
- Images are transformed from color domain to depth domain using satellite-derived bathymetry
- Invisible submerged targets to human eyes are detected based on depth anomalies

Supporting Information:

Supporting Information may be found in the online version of this article.

Correspondence to:

Y. Ma,
mayue_eis@whu.edu.cn

Citation:

Liu, H., Yang, J., Ma, Y., Li, Y., & Wang, X. H. (2025). Detection of submerged targets beyond eyes' observation using satellite lidar and multispectral data. *Geophysical Research Letters*, *52*, e2025GL118498. https://doi.org/10.1029/2025GL118498

Received 28 JUL 2025
Accepted 29 OCT 2025

Author Contributions:

Conceptualization: Hao Liu, Jian Yang, Yue Ma
Data curation: Jian Yang
Funding acquisition: Jian Yang, Yue Ma, Yao Li
Investigation: Hao Liu, Yue Ma, Yao Li
Methodology: Hao Liu, Jian Yang
Project administration: Yue Ma, Xiao Hua Wang
Supervision: Yue Ma, Yao Li, Xiao Hua Wang
Validation: Hao Liu, Jian Yang
Writing – original draft: Hao Liu, Jian Yang
Writing – review & editing: Yue Ma, Yao Li, Xiao Hua Wang

Abstract Detecting submerged targets in shallow waters from satellite platforms remains a challenge, as the optical spectral information of targets is significantly distorted by the absorption and scattering effects of the water column. In this study, we propose a new framework as the bathymetry-informed target extraction, which integrates the spaceborne lidar data and multispectral imagery. By using lidar assisted Satellite-Derived Bathymetry model, we convert the complex multispectral information into relative depth data. Through this transformation, the challenging issue of distorted color domain image segmentation is converted into the task of depth anomaly detection. The method is validated on submerged artificial stone weirs and breakwaters in typical open ocean and coastal waters, which indicates significant improvements in target detection rate and reliability compared to direct color-based methods. This approach promises large-scale surveys of submerged targets in shallow waters, offering an alternative solution to on-site surveys such as shipborne sonars.

Plain Language Summary Finding and locating the objects underwater from satellites has a great demand for marine surveying and navigation safety, but it is one of the most challenging tasks in remote sensing. An important reason is that the color information of light may be significantly distorted when it travels through the water column before being reflected by targets, making it nearly impossible for common target detection algorithms to extract features. To overcome this problem, we developed a new method that, for the first time, successfully detects submerged objects only using satellite data. Instead of relying on color differences in the image, which is accustomed to our human eyes, our approach uses satellite derived bathymetry that transforms the color image into a three-dimensional seabed map in shallow water. The depth differences among adjacent pixels in the map clearly expose the underwater objects, which are not visible to our eyes. This method is validated in typical open ocean and coastal waters and using satellite images and laser points, and we successfully found all known underwater stone weirs. This breakthrough could significantly expand what satellites can detect beneath the ocean surface in the future.

1. Introduction

The detection of submerged targets holds significant importance for marine surveying and navigation safety (Zhang, Xing, et al., 2024, Zhang, Yang & Yang, 2024). Currently, the detection of submerged targets primarily relies on shipborne and underwater platform based techniques (Feng et al., 2024), including shipborne sonar, multibeam echosounder, hyperspectral imaging measurements, and underwater multispectral imaging (Bruno et al., 2011; Menna et al., 2018). By actively emitting acoustic waves and receiving their echoes, shipborne sonar and multibeam echosounder systems can accurately map bottom topography and detect protruding targets relative to the surrounding seabed (Long et al., 2023; Yang et al., 2011). Meanwhile, with high spatial resolution better than the decimeter level, on-site hyperspectral imagery measurements of water surface remote sensing reflectance have become an important approach to retrieve the water depths and boundaries of submerged targets (Doan et al., 2022; Li et al., 2023). To further minimize the effects of sea surface waves and reduce the influence of the water column, underwater imaging devices have been employed for high-precision detection of submerged targets and topography (Li et al., 2025; Yuan et al., 2022). Although these techniques provide abundant observation methods and accurate underwater information, it is hampered by vessel accessibility, rendering them impractical for remote marine areas or hazardous marine environments.

Over past decades, satellite remote sensing techniques have provided cost-effective observation data at a global scale, revolutionizing our understanding of aquatic and terrestrial systems (Behrenfeld et al., 2019; Churnside &

Marchbanks, 2015; Magruder et al., 2024; O'Malley et al., 2014). With the advancement of satellite image processing algorithms, the image-based detection of terrestrial targets has become a mature and efficient way, which primarily relies on the significant differences in spectral (color) and textural features between the target and its background pixels (Li et al., 2020; McCarthy et al., 2018). However, significant physical challenges exist when the satellite image processing framework is directly transposed to underwater environments (Dumke et al., 2018; Telem & Filin, 2013). Due to the strong absorption and scattering effects in the water column, light intensity rapidly decreases with the rising water depth and varies across wavelengths (Wang et al., 2022; Werdell et al., 2013). This leads to significant distortion of the spectral information from submerged targets (Lee et al., 1998), and the satellite derived reflectance (or remote sensing reflectance) is no longer dominated by the spectral characteristics of the target, making methods that solely rely on spectral and brightness information exceptionally challenging for target detection.

Generally, target detection based on remote sensing optical imagery requires targets to possess distinctive color characteristics from the background. However, two challenges always arise in discerning these color differences in underwater scenarios: (a) the surroundings are spectrally complex, which overwhelms the distorted target spectral information, and (b) the target is indistinguishable due to the significant attenuation in the water column. Currently, the data-driven methods (e.g., deep learning) directly applied to optical imagery cannot effectively resolve this issue, as human observers struggle to detect the target in the above cases, thus failing to provide a reliable truth label for training. Therefore, a novel framework for achieving underwater target detection is urgently needed. Acoustic-based submerged target detection has demonstrated the feasibility of detecting targets based on relative depth variations rather than relying on radiometric signatures.

Satellite Derived Bathymetry (SDB) is a technique that estimates the water depth for each pixel in remote sensing imagery which has been extensively investigated and refined over the past few decades (Armon et al., 2020; Kutser et al., 2020). Typically, SDB can achieve bathymetric measurements of several meters in coastal waters and 20–30 m in open ocean waters, and it has an accuracy of better than 10% of the maximum depth (Ashphaq et al., 2021; Kutser et al., 2020). The photon-counting lidar on Ice, Cloud and land Elevation Satellite-2 (ICESat-2) has further enhanced the capabilities of SDB (Markus et al., 2017; Parrish et al., 2019) and enables the global bathymetric mapping without on-site depth seeds (Babbel et al., 2021; Ma et al., 2020; Thomas et al., 2021; Xie et al., 2021; Zhang, Xing, et al., 2024, Zhang, Yang & Yang, 2024). This lidar-assisted SDB has created an opportunity to find protrusions in the sea floor, which works as a means of submerged target detection solely from satellite observations.

The target and environment induced spectral information is usually imperceptible in the original optical imagery. In this study, to avoid the issue of directly processing spectral distorted images, a new framework of submerged target detection is proposed and named as bathymetry-informed target extraction (BITE). The core of this framework lies in lidar assisted SDB, which compresses and remaps a multiple-band optical image into one-band bathymetric image. Specifically, the wavelength-dependent attenuation patterns of light in water are transformed into depth information, meaning that subtle differences in multiple color channels are "compressed" into only one channel, that is, the distinguishable depths. Through this transformation, the challenging problem of distorted color domain image segmentation is converted into a problem of depth anomaly detection. Theoretically, leveraging SDB for submerged target extraction in shallow waters has the potential to achieve results comparable to those of shipborne acoustic-based detection. With the derived bathymetric map, we further use a practical and efficient salient target detection model to achieve automated and training-free extraction of submerged targets.

2. Materials

To achieve the detection of submerged targets, this study integrated both lidar and optical data sources on satellite platforms. (a) Optical remote sensing imagery: this study utilized multispectral imagery from Beijing-3 and Sentinel-2 satellite. The Beijing-3 data feature four spectral bands (i.e., blue, green, red, and near-infrared band) and a spatial resolution of 2 m (Yang, Jian, et al., 2023, Yang, Ma, et al., 2023), while the Sentinel-2 data have similar four bands with a resolution of 10 m (Drusch et al., 2012). The imagery provided the spectral information sufficient for constructing the SDB model and was used to generate a comprehensive bathymetric map of each entire study site. (b) Photon-counting lidar points: this study utilized all available ATL03 data, generated by the Advanced Topographic Laser Altimeter System aboard NASA's Ice, Cloud, and land Elevation Satellite-2 (ICESat-2) (Neumann et al., 2023). High-accuracy bathymetric points were extracted from raw noisy point

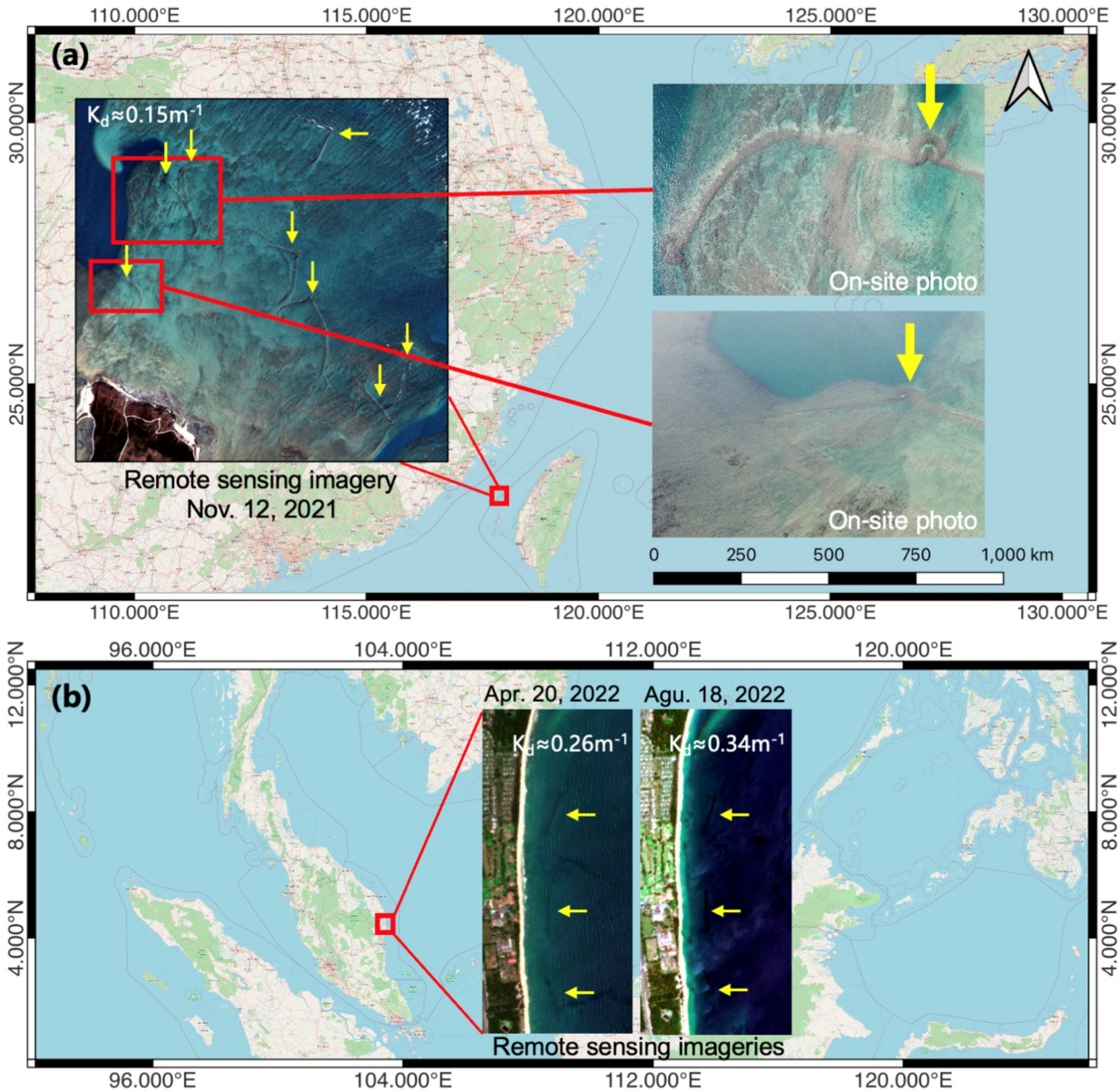

Figure 1. Schematic diagram of the study area and some cases of submerged targets. (a) In Penghu Islands; (b) in Kuala Dungun. The inset remote sensing imagery in (a) corresponds to the subfigure Figure 3a, while inset remote sensing imageries in (b) correspond to Figures 3d and 3f.

data, which underwent a process of automated classification, denoising, and correction for underwater bathymetric errors (Babbel et al., 2021; Chen et al., 2021; Fricker et al., 2021; Ma et al., 2020; Parrish et al., 2019). These bathymetric points were essential for training the SDB model.

In Figure 1a, the first study area is Penghu Islands, China, located in Taiwan Strait at approximately 23.590°N, 119.671°E, with the SDB derived depth range of 0–12 m. The annual mean diffuse attenuation coefficient K_d is ∼0.15 m^{-1} with seasonal variations of ∼0.10–0.17 m^{-1} belonging to Case I open ocean waters (Mobley, 1994). The nearshore seabed substrate consists of silt and dark sand, and the tidal range is ∼2.0 m. There are many stone weirs near the coast, providing three independent sites for validation. Structurally, the stone weir consists of an arc-shaped stone dike, which has a width of approximately 4–8 m and extends from shallow to deep waters. These stone weirs possess a distinct physical height, typically rising 0.5–1.5 m above the surrounding seabed, which constitutes a clear topographic anomaly. The geographic coordinates for some of these weirs can be obtained from

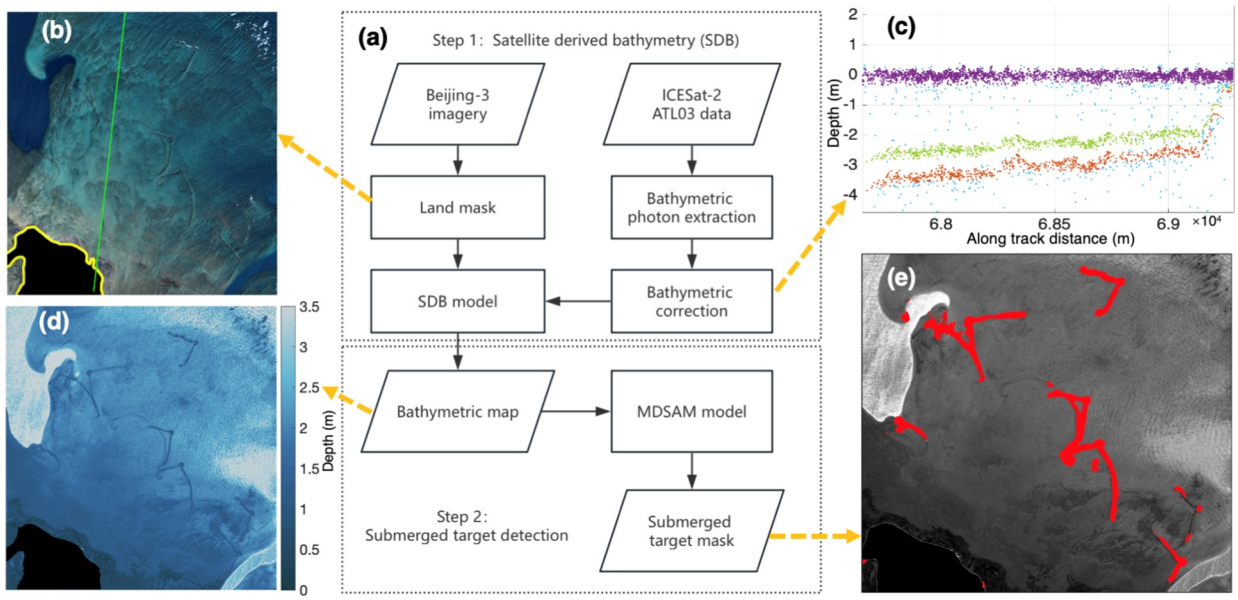

Figure 2. (a) Workflow diagram; (b)–(e) intermediate results of submerged artificial targets detected using the bathymetry-informed target extraction framework. Specifically, (b) satellite optical images after applying land mask where the black area with a yellow edge represents land and the green line represents the ICESat-2 track shown in (c). (c) ICESat-2 bathymetric points after type classification and bathymetric correction, where the purple points represent the water surface, the red points represent the seabed, and the green points represent the seabed after bathymetric correction. (d) Derived satellite-derived bathymetry map in Step (1). (e) Submerged artificial targets which are automatically detected using multi-scale and detail-enhanced segment anything model.

the Penghu stone weir information platform (https://stoneweir.info). Beijing-3 imagery captured on 2021/11/12 when the seasonal mean K_d is 0.15 m^{-1} was employed to detect these stone weirs.

In Figure 1b, the second study area is Kuala Dungun, Malaysia, located at approximately 4.414°N, 103.442°E, with the SDB depth range of 0–6 m. The annual mean K_d is ~0.33 m^{-1} belonging to Case II coastal waters, which is much more turbid than that in Penghu Islands. Kuala Dungun exhibits significant seasonal fluctuations, with K_d around 0.25 m^{-1} in the first two quarters, increasing to 0.34 m^{-1} in the third quarter, and sharply rising to 0.76 m^{-1} in the fourth quarter. The nearshore seabed substrate consists of bright sand, and the tidal range is ~1.9 m. There are three submerged breakwaters designed to reduce wave energy and mitigate coastal erosion of the Kerteh town shoreline. These breakwaters are placed on the seabed at a depth of approximately 4 m relative to local mean sea level, with a height of ~2 m above the seabed (Teh & Hashim, 2014). The three breakwaters have a length of hundreds of meters and a width of nearly 30 m located 300 m offshore. Sentinel-2 imageries were employed here and captured on 2022/04/20 and 2022/08/18 corresponding the seasonal mean K_d of 0.26 m^{-1} and 0.34 m^{-1}.

3. Methodology

The proposed BITE framework for submerged target detection is illustrated in Figure 2a. The first step of this framework involves transforming the pixel data of satellite imagery from the color domain to a domain representing relative bathymetric variations, which was achieved by an active-passive fusion bathymetry inversion approach (Ma et al., 2020; Zhuang et al., 2022). The second step of the framework is to perform submerged target detection based on the generated relative bathymetry map, for which we have conducted a submerged target detection algorithm.

The first step comprises the workflow for generating a SDB map by fusing ICESat-2 bathymetric points with Beijing-3 or Sentinel-2 spectral imagery. Specifically, an improved adaptive Density-Based Spatial Clustering of Applications with Noise algorithm is employed to separate the sea surface and seafloor signal points from ATL03 raw noisy points (Parrish et al., 2022). The refraction effect at the air-water interface and in the water column, as well as the scattering effect in the water column, are sequentially corrected using ICESat-2's sea surface and water backscattering data (Parrish et al., 2019; Shangguan et al., 2025; Yang, Jian, et al., 2023, Yang, Ma, et al., 2023; Zheng et al., 2025). An example of the point classification and bathymetric correction is illustrated in Figure 2c.

By incorporating local tidal information from FES2014 model (Carrere et al., 2015; Wang et al., 2023), the vertical datum of ICESat-2 derived bathymetric points is transformed into the local depth datum. Through these steps, the seed depths from ICESat-2 bathymetric points are obtained.

Then, for Beijing-3 and Sentinel-2 multispectral imagery, the Normalized Difference Water Index is calculated to mask and filter out the pixels covered by clouds and located on land (B. Gao, 1996), thereby retaining only water pixels. The mask boundaries are highlighted in yellow curves in Figure 2b. By applying a projection algorithm, the coordinates of ICESat-2 seed points are transformed into the projection coordinate system of remote sensing imagery. Then, ICESat-2 seed points are matched with the corresponding geographic pixels in the imagery. This process results in the construction of a SDB data set, where four band remote sensing reflectance values correspond to one depth value. Many algorithms have been proposed to derive SDB models (Albright & Glennie, 2021; Armon et al., 2020; Caballero & Stumpf, 2023; Dekker et al., 2011; Hsu et al., 2021; Lyzenga, 1985; Manessa et al., 2016; Peng et al., 2022; Stumpf et al., 2003; Thomas et al., 2021).

In this study, we used three algorithms which represent the physics-based linear band model (Lyzenga et al., 2006), machine learning-based random forest algorithm (RF) model (Mudiyanselage et al., 2022), and deep learning-based physics-assisted convolutional neural network model (Peng et al., 2022). The depth seed points were randomly divided into training and validation subsets to separately train and evaluate the model, where ten-fold cross-validation is applied to verify the accuracy. Here, the root mean square error and R-square between the validation seed depths and their corresponding estimated depths is used to assess the performance (Chai & Draxler, 2014). Using three SDB algorithms, the trained models which link the remote sensing reflectance with water depths are applied to the entire image and then produce the bathymetric map of each study site, where an example is shown in Figure 2d.

As potential submerged targets normally lack fixed shapes or common features, we utilize a salient target detection algorithm, which can automatically detect and focus on the most eye-catching or "unusual" areas within an image (Borji et al., 2019). Specifically, a deep learning-based target detection model, Multi-Scale and Detail-Enhanced Segment Anything Model (MDSAM), is used (S. Gao et al., 2024). MDSAM integrates salient target detection and Segment Anything Model (Kirillov et al., 2023), which can segment any targets within the image without training for specific tasks. In Step (b), the bathymetric map is linearly normalized into a grayscale image ranging from 0 to 255 Gy levels, where the gray level 0 corresponds to the deepest depth and 255 corresponds to the sea surface (0 m). This grayscale image is then used as the input to MDSAM. The heatmap output by MDSAM is binarized using Otsu's thresholding method (Otsu, 1979) to obtain a binary mask, and some extracted targets are labeled by red marks in Figure 2e as examples. Precision, Recall, and F_1 score are used as the metrics to evaluate the BITE detection performance (Sokolova & Lapalme, 2009).

4. Results

The results are presented in two steps: (a) the enhancement of submerged target detectability through SDB, and (b) the performance of submerged target labeling using the MDSAM model. In Step (a), the detailed model construction and validation results are in Text and Figure S1 in Supporting Information S1, which indicates three SDB algorithms achieve relatively similar performance. In subsequent experiments, we adopted the RF model, which balances the accuracy and complexity, as the method for SDB. Three sites from Penghu Islands are presented in Figures 3a–3c, which illustrate typical challenges in detecting shallow-water submerged targets from remote sensing imagery. Figure 3a involves the targets, which are visible to human eyes but are difficult to automatically extract due to highly complex backgrounds. Specifically, the submerged target is situated at a depth of approximately 1–2 m, surrounded by sediments and rocks which exhibit spectral colors similar to the targets. The targets in Figures 3b and 3c are located at depths of 3–6 m, which are nearly imperceptible to human eyes because the slight color variations among adjacent pixels are nearly undetectable in the imagery.

One site in Kuala Dungun is shown in Figures 3d and 3e, where submerged targets are located at depths of 2–3 m and the seasonal variations of water qualities are considered. Due to coastal water conditions, these targets are likewise difficult to directly observe from remote sensing images, especially in Figure 3e. In contrast, the SDB map amplifies the discrepancy among adjacent pixels through the depth differences, as shown in Figures 3f–3j. As shown in Figure 3f, the spectrally complex background is transformed into a combination of a nearly uniform background and a prominent object, and the submerged target clearly arises. In Figures 3g–3j, after SDB inversion, the targets are significantly enhanced against the surrounding seabed, revealing a clear outline and

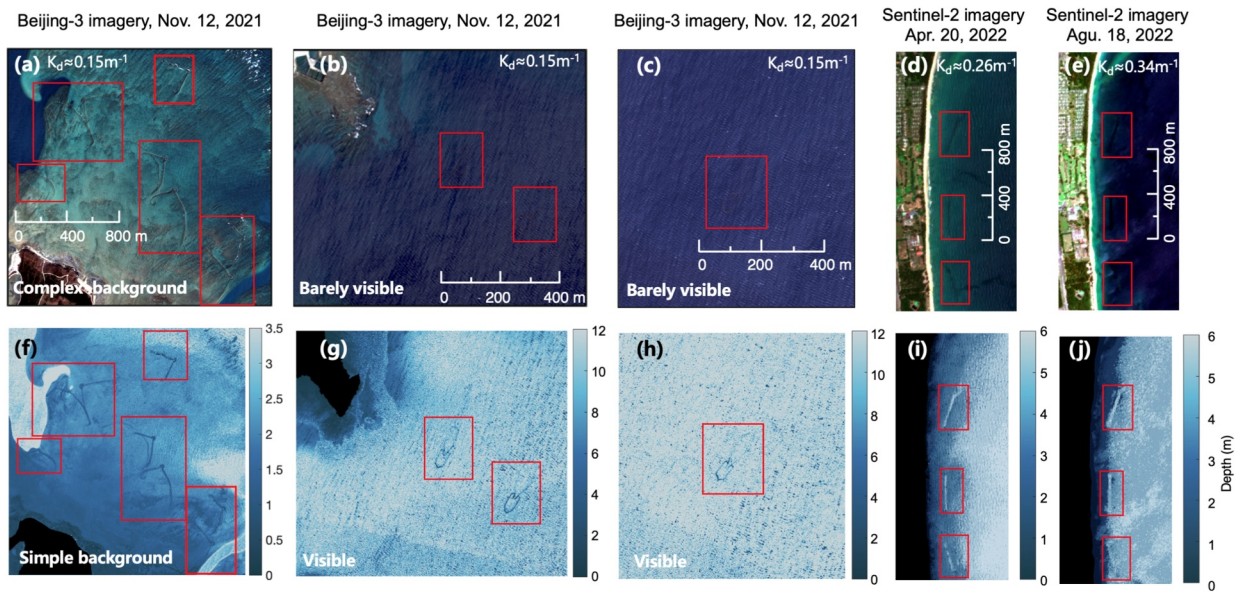

Figure 3. Satellite-derived bathymetry (SDB) maps and their preliminary detection for submerged targets. (a)–(c) Original remote sensing color imageries from Beijing-3 in Penghu islands; (d)–(e) Original color imagery from Sentinel-2 in Kuala Dungun considering seasonal variations of water qualities; (f)–(j) the corresponding SDB maps of (a)–(e). The red box indicates the locations of submerged targets.

features indicative of an artificial structure. However, comparing Figures 3i and 3j, worse water qualities have an impact on the protrusion feature and may further influence the target detection. In summary, the SDB transformation significantly enhances the submerged target detectability and renders even optically obscured targets distinguishable to the human eye.

Then, in Step (b), the SDB maps are input into the MDSAM model to conduct submerged target detections. In Figure 4, based on the local reference data, we manually annotate ground-truth labels on SDB maps using green markers. Figures 4a–4e indicate that all submerged targets are successfully detected by BITE. As contrast, the red markers in Figures 4f–4j present the results obtained by directly applying MDSAM to multispectral remote sensing imagery rather than firstly transforming into SDB map. In Figure 4f, only three complete profiles and a partial profile of stone weirs are detected. The results in Figures 4g–4j indicate that the MDSAM model struggles to extract low color contrast targets which are also imperceptible to human eyes in original optical images. Across all SDB-based detections, the MDSAM model exhibits good detection performance and barely any misjudgments.

The quantitative analysis indicates the detection precisions range from 47% to 89%, recalls from 74% to 92%, and F_1 scores from 0.50 to 0.90. Specifically, Site 2 achieved the best performance (Precision: 89%, Recall: 92%, and F_1: 0.90), while Site 4 with bad water quality showed lower precision (Precision: 47%). One reason is that, the SDB accuracy is strongly correlated with water quality. In turbid waters, inversion uncertainty significantly increases, which substantially impedes the framework's ability to detect complete target structures. This lower precision is also caused by the MDSAM computation involving downsampling and upsampling, introducing the detected contours wider than the ground-truth annotations. This also leads to the recall values being consistently higher than their corresponding precision values across all study sites. Such a trend reflects the conservative bias of the detection process, favoring the inclusiveness to ensure that potential targets are not missed. In practical applications, this characteristic is beneficial to surveying submerged structures, since omission errors (false negatives) are generally more detrimental than commission errors (false positives).

5. Discussion

The applicability of the BITE method primarily depends on two key factors: (a) the spatial resolution of satellite imageries and (b) the environmental conditions, including water quality and target reflectance. The imagery spatial resolution is a critical constraint influencing underwater target detection. This stems from the fundamental

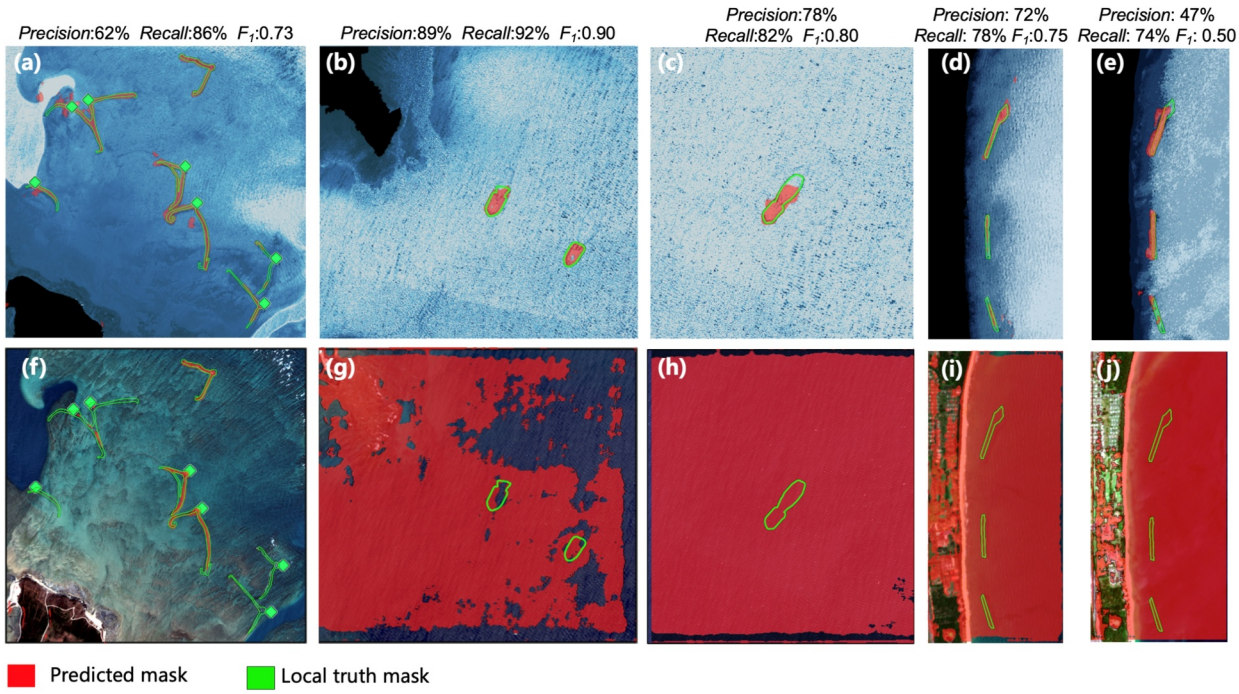

Figure 4. Results of submerged target detections. (a)–(e) Target detection using multi-scale and detail-enhanced segment anything model (MDSAM) from satellite-derived bathymetry maps, that is, using BITE; (f)–(j) target detection using MDSAM from original color imagery. The green markers represent the mask of submerged target regions based on local reference data, and the red marks represent the mask of submerged target regions detected by MDSAM.

requirement that a target must exhibit distinct spatial features within the imagery to be reliably detected. The BITE framework also needs to follow the basic rule of detecting targets from images, that is, the smallest size of a target should be at least twice or three times than the spatial resolution of the used image (Blaschke, 2010; Early & Long, 2001). This guideline ensures that the target covers multiple pure pixels, thereby mitigating significant signal contamination from the mixed pixel effect and allowing for the unambiguous confirmation of the target's outline and presence. In the Text S2 and Figure S2 in Supporting Information S1, we list a quantitative comparison of submerged targets observed by Sentinel-2 and Beijing-3 imageries.

BITE operates most effectively in clear and shallow waters where sufficient light penetration through the water column is possible. Better water clarity (i.e., smaller K_d) allows for greater maximum depths in SDB, consequently extending the operational depth of the BITE framework. A detailed discussion on the maximum effective depth of different environmental conditions and the seasonal variations of water qualities is provided in the Texts S3 and S4 and Figures S3 and S4 in Supporting Information S1, and here is a brief conclusion. The environmental adaptability of the BITE framework is limited by both water quality and target reflectivity. Under ideal conditions (e.g., white coral reef bottom of $R_b \approx 0.4$ and very clear water of $K_d \approx 0.058$ m^{-1}), the detection limit using Sentinel-2 data can theoretically reach ~20 m. However, in more typical coastal water environments and artificial submerged targets such as Penghu ($K_d \approx 0.15$ m^{-1}, $R_b \approx 0.2$) and Kuala Dungun ($K_d \approx 0.34$ m^{-1}, $R_b \approx 0.2$), the effective depth decreases sharply to 8.4 and 3.7 m, respectively. In Penghu islands and Kuala Dungun, the artificial submerged targets are located in depths of 3–6 m and 2–3 m, respectively, which are generally in accordance with the depth limits of theoretical predictions. These results imply that the BITE framework is unlikely to succeed in extreme cases of turbid waters, where the signal-to-noise ratio is insufficient for stable detection. Consequently, the applicability of the framework should be considered restricted to Case I open ocean and Case II coastal waters (Mobley, 1994).

6. Conclusions

This study proposes and validates a novel framework for detecting shallow-water submerged targets from satellite lidar points and optical imagery, named BITE. The main concept is the "dimensionality transformation", which utilizes the lidar assisted SDB technique to "compress" the complex multispectral information in color images

and remap it onto depth data. This process simplifies a challenging image segmentation problem to a more straightforward depth anomaly detection task.

In practice, the absolute accuracy of SDB is not the primary factor for target detection, but the relative depth differences among adjacent pixels are the key point, as long as the SDB model can roughly reflect the "protrusion" of the submerged target relative to its surrounding seabed. Therefore, we recommend using any feasible SDB algorithm to conduct this framework. To highlight the target detection process in BITE, we select a zero-shot deep learning model, MDSAM, which requires no annotation or training. Even if the absolute depth values from the SDB transformation are not perfectly accurate, this final detection of submerged targets remain solid in the experiments.

Compared to shipborne sonars and multibeam echosounders, the proposed BITE framework enables large-scale submerged target surveys of extensive and shallow sea areas. Nevertheless, this framework does have some limitations, mainly limited to the water clarity. In turbid waters, the penetration depth of SDB is severely limited. Furthermore, as MDSAM is a generic salient target detection model, its output may not perfectly align with the specific geometric shapes of targets. Future works may explore the use of SDB data to fine-tune deep learning models to further improve their accuracy and robustness in submerged target segmentation.

Conflict of Interest

The authors declare no conflicts of interest relevant to this study.

Data Availability Statement

The used ICESat-2 data are available on NSIDC website (Neumann et al., 2023), the procedure and result data sets are available on a specific Zenodo website (Liu et al., 2025), and the on-site reference data are available on https://stoneweir.info.

Acknowledgments
This work was supported in part by the National Natural Science Foundation of China under Grants 42371440 and 42201349 and the China Postdoctoral Science Foundation under Grants GZB20240563 and 2025M770249. We gratefully acknowledge the National Snow and Ice Data Center (NSIDC) for providing the ICESat-2 ATL03 product (https://nsidc.org/data/atl03/versions/6) and the Penghu stone weir information platform providing on-site photographs and coordinates of stone weirs (https://stoneweir.info).

References

Albright, A., & Glennie, C. (2021). Nearshore bathymetry from fusion of Sentinel-2 and ICESat-2 observations. *IEEE Geoscience and Remote Sensing Letters*, *18*(5), 900–904. https://doi.org/10.1109/LGRS.2020.2987778

Armon, M., Dente, E., Shmilovitz, Y., Mushkin, A., Cohen, T. J., Morin, E., & Enzel, Y. (2020). Determining bathymetry of shallow and ephemeral desert Lakes using satellite imagery and altimetry. *Geophysical Research Letters*, *47*(7), e2020GL087367. https://doi.org/10.1029/2020GL087367

Ashphaq, M., Srivastava, P. K., & Mitra, D. (2021). Review of near-shore satellite derived bathymetry: Classification and account of five decades of coastal bathymetry research. *Journal of Ocean Engineering and Science*, *6*(4), 340–359. https://doi.org/10.1016/j.joes.2021.02.006

Babbel, B. J., Parrish, C. E., & Magruder, L. A. (2021). ICESat-2 elevation retrievals in support of satellite-derived bathymetry for global science applications. *Geophysical Research Letters*, *48*(5), e2020GL090629. https://doi.org/10.1029/2020GL090629

Behrenfeld, M. J., Gaube, P., Della Penna, A., O'Malley, R. T., Burt, W. J., Hu, Y., et al. (2019). Global satellite-observed daily vertical migrations of ocean animals. *Nature*, *576*(7786), 257–261. https://doi.org/10.1038/s41586-019-1796-9

Blaschke, T. (2010). Object based image analysis for remote sensing. *ISPRS Journal of Photogrammetry and Remote Sensing*, *65*(1), 2–16. https://doi.org/10.1016/j.isprsjprs.2009.06.004

Borji, A., Cheng, M.-M., Hou, Q., Jiang, H., & Li, J. (2019). Salient object detection: A survey. *Computational Visual Media*, *5*(2), 117–150. https://doi.org/10.1007/s41095-019-0149-9

Bruno, F., Bianco, G., Muzzupappa, M., Barone, S., & Razionale, A. V. (2011). Experimentation of structured light and stereo vision for underwater 3D reconstruction. *ISPRS Journal of Photogrammetry and Remote Sensing*, *66*(4), 508–518. https://doi.org/10.1016/j.isprsjprs.2011.02.009

Caballero, I., & Stumpf, R. P. (2023). Confronting turbidity, the major challenge for satellite-derived coastal bathymetry. *Science of The Total Environment*, *870*, 161898. https://doi.org/10.1016/j.scitotenv.2023.161898

Carrere, L., Lyard, F., Cancet, M., & Guillot, A. (2015). *FES 2014, a new tidal model on the global ocean with enhanced accuracy in shallow seas and in the arctic region* (Vol. 5481). EGU General Assembly Conference Abstracts.

Chai, T., & Draxler, R. R. (2014). Root mean square error (RMSE) or mean absolute error (MAE)? – Arguments against avoiding RMSE in the literature. *Geoscientific Model Development*, *7*(3), 1247–1250. https://doi.org/10.5194/gmd-7-1247-2014

Chen, Y., Zhu, Z., Le, Y., Qiu, Z., Chen, G., & Wang, L. (2021). Refraction correction and coordinate displacement compensation in nearshore bathymetry using ICESat-2 lidar data and remote-sensing images. *Optics Express*, *29*(2), 2411–2430. https://doi.org/10.1364/OE.409941

Churnside, J. H., & Marchbanks, R. D. (2015). Subsurface plankton layers in the Arctic Ocean. *Geophysical Research Letters*, *42*(12), 4896–4902. https://doi.org/10.1002/2015GL064503

Dekker, A. G., Phinn, S. R., Anstee, J., Bissett, P., Brando, V. E., Casey, B., et al. (2011). Intercomparison of shallow water bathymetry, hydro-optics, and benthos mapping techniques in Australian and Caribbean coastal environments: Intercomparison of shallow water mapping methods. *Limnology and Oceanography: Methods*, *9*(9), 396–425. https://doi.org/10.4319/lom.2011.9.396

Doan, V.-S., Huynh-The, T., & Kim, D.-S. (2022). Underwater acoustic target classification based on dense convolutional neural network. *IEEE Geoscience and Remote Sensing Letters*, *19*, 1–5. https://doi.org/10.1109/LGRS.2020.3029584

Drusch, M., Del Bello, U., Carlier, S., Colin, O., Fernandez, V., Gascon, F., et al. (2012). Sentinel-2: eSA's optical high-resolution mission for GMES operational services. *Remote Sensing of Environment*, *120*, 25–36. https://doi.org/10.1016/j.rse.2011.11.026

Dumke, I., Nornes, S. M., Purser, A., Marcon, Y., Ludvigsen, M., Ellefmo, S. L., et al. (2018). First hyperspectral imaging survey of the deep seafloor: High-resolution mapping of manganese nodules. *Remote Sensing of Environment*, *209*, 19–30. https://doi.org/10.1016/j.rse.2018.02.024

Early, D. S., & Long, D. G. (2001). Image reconstruction and enhanced resolution imaging from irregular samples. *IEEE Transactions on Geoscience and Remote Sensing*, *39*(2), 291–302. https://doi.org/10.1109/36.905237

Feng, S., Zhu, X., & Ma, S. (2024). Masking hierarchical tokens for underwater acoustic target recognition with self-supervised learning. *IEEE/ACM Transactions on Audio, Speech, and Language Processing*, *32*, 1365–1379. https://doi.org/10.1109/TASLP.2024.3358719

Fricker, H. A., Arndt, P., Brunt, K. M., Datta, R. T., Fair, Z., Jasinski, M. F., et al. (2021). ICESat-2 meltwater depth estimates: Application to surface melt on amery ice shelf, east Antarctica. *Geophysical Research Letters*, *48*(8), e2020GL090550. https://doi.org/10.1029/2020GL090550

Gao, B. (1996). NDWI—A normalized difference water index for remote sensing of vegetation liquid water from space. *Remote Sensing of Environment*, *58*(3), 257–266. https://doi.org/10.1016/S0034-4257(96)00067-3

Gao, S., Zhang, P., Yan, T., & Lu, H. (2024). Multi-scale and detail-enhanced segment anything model for salient object detection. In *Proceedings of the 32nd ACM international conference on multimedia* (pp. 9894–9903). ACM. https://doi.org/10.1145/3664647.3680650

Hsu, H.-J., Huang, C.-Y., Jasinski, M., Li, Y., Gao, H., Yamanokuchi, T., et al. (2021). A semi-empirical scheme for bathymetric mapping in shallow water by ICESat-2 and Sentinel-2: A case study in the South China Sea. *ISPRS Journal of Photogrammetry and Remote Sensing*, *178*, 1–19. https://doi.org/10.1016/j.isprsjprs.2021.05.012

Kirillov, A., Mintun, E., Ravi, N., Mao, H., Rolland, C., Gustafson, L., et al. (2023). Segment anything. *arXiv*, 3992–4003. https://doi.org/10.1109/iccv51070.2023.00371

Kutser, T., Hedley, J., Giardino, C., Roelfsema, C., & Brando, V. E. (2020). Remote sensing of shallow waters – A 50 year retrospective and future directions. *Remote Sensing of Environment*, *240*, 111619. https://doi.org/10.1016/j.rse.2019.111619

Lee, Z., Carder, K. L., Mobley, C. D., Steward, R. G., & Patch, J. S. (1998). Hyperspectral remote sensing for shallow waters I A semianalytical model. *Applied Optics*, *37*(27), 6329. https://doi.org/10.1364/AO.37.006329

Li, H., Wang, H., Zhang, Y., Li, L., & Ren, P. (2025). Underwater image captioning: Challenges, models, and datasets. *ISPRS Journal of Photogrammetry and Remote Sensing*, *220*, 440–453. https://doi.org/10.1016/j.isprsjprs.2024.12.002

Li, K., Wan, G., Cheng, G., Meng, L., & Han, J. (2020). Object detection in optical remote sensing images: A survey and a new benchmark. *ISPRS Journal of Photogrammetry and Remote Sensing*, *159*, 296–307. https://doi.org/10.1016/j.isprsjprs.2019.11.023

Li, Q., Li, J., Li, T., Li, Z., & Zhang, P. (2023). Spectral–spatial depth-based framework for hyperspectral underwater target detection. *IEEE Transactions on Geoscience and Remote Sensing*, *61*, 1–15. https://doi.org/10.1109/TGRS.2023.3275147

Liu, H., Yang, J., & Ma, Y. (2025). Detection of submerged targets beyond eyes' observation using satellite Lidar and multispectral data [Dataset]. *Zenodo*. https://doi.org/10.5281/zenodo.15845481

Long, H., Shen, L., Wang, Z., & Chen, J. (2023). Underwater forward-looking sonar images target detection via speckle reduction and scene prior. *IEEE Transactions on Geoscience and Remote Sensing*, *61*, 1–13. https://doi.org/10.1109/TGRS.2023.3248605

Lyzenga, D. R. (1985). Shallow-water bathymetry using combined lidar and passive multispectral scanner data. *International Journal of Remote Sensing*, *6*(1), 115–125. https://doi.org/10.1080/01431168508948428

Lyzenga, D. R., Malinas, N. P., & Tanis, F. J. (2006). Multispectral bathymetry using a simple physically based algorithm. *IEEE Transactions on Geoscience and Remote Sensing*, *44*(8), 2251–2259. https://doi.org/10.1109/TGRS.2006.872909

Ma, Y., Xu, N., Liu, Z., Yang, B., Yang, F., Wang, X. H., & Li, S. (2020). Satellite-derived bathymetry using the ICESat-2 lidar and Sentinel-2 imagery datasets. *Remote Sensing of Environment*, *250*, 112047. https://doi.org/10.1016/j.rse.2020.112047

Magruder, L. A., Farrell, S. L., Neuenschwander, A., Duncanson, L., Csatho, B., Kacimi, S., & Fricker, H. A. (2024). Monitoring Earth's climate variables with satellite laser altimetry. *Nature Reviews Earth and Environment*, *5*(2), 120–136. https://doi.org/10.1038/s43017-023-00508-8

Manessa, M. D. M., Kanno, A., Sekine, M., Haidar, M., Yamamoto, K., Imai, T., & Higuchi, T. (2016). Satellite-drived bathymetry using random forest algorithm and Worldview-2 imagery. *Geoplanning: Journal of Geomatics and Planning*, *3*(2), 117. https://doi.org/10.14710/geoplanning.3.2.117-126

Markus, T., Neumann, T., Martino, A., Abdalati, W., Brunt, K., Csatho, B., et al. (2017). The ice, cloud, and land elevation Satellite-2 (ICESat-2): Science requirements, concept, and implementation. *Remote Sensing of Environment*, *190*, 260–273. https://doi.org/10.1016/j.rse.2016.12.029

McCarthy, M. J., Radabaugh, K. R., Moyer, R. P., & Muller-Karger, F. E. (2018). Enabling efficient, large-scale high-spatial resolution wetland mapping using satellites. *Remote Sensing of Environment*, *208*, 189–201. https://doi.org/10.1016/j.rse.2018.02.021

Menna, F., Agrafiotis, P., & Georgopoulos, A. (2018). State of the art and applications in archaeological underwater 3D recording and mapping. *Journal of Cultural Heritage*, *33*, 231–248. https://doi.org/10.1016/j.culher.2018.02.017

Mobley, C. D. (1994). *Light and water: Radiative transfer in natural waters*. Academic Press. Retrieved from http://archive.org/details/lightwaterradiat0000mobl

Mudiyanselage, S. S. J. D., Abd-Elrahman, A., Wilkinson, B., & Lecours, V. (2022). Satellite-derived bathymetry using machine learning and optimal Sentinel-2 imagery in south-west Florida coastal waters. *GIScience and Remote Sensing*, *59*(1), 1143–1158. https://doi.org/10.1080/15481603.2022.2100597

Neumann, T. A., Brenner, A., Hancock, D., Robbins, J., Gibbons, A., Lee, J., et al. (2023). ATLAS/ICESat-2 L2A global geolocated photon data. (ATL03, version 6) [Dataset]. *NASA National Snow and Ice Data Center Distributed Active Archive Center*. https://doi.org/10.5067/ATLAS/ATL03.006

O'Malley, R. T., Behrenfeld, M. J., Westberry, T. K., Milligan, A. J., Shang, S., & Yan, J. (2014). Geostationary satellite observations of dynamic phytoplankton photophysiology. *Geophysical Research Letters*, *41*(14), 5052–5059. https://doi.org/10.1002/2014GL060246

Otsu, N. (1979). A threshold selection method from gray-level histograms. *IEEE Transactions on Systems, Man, and Cybernetics*, *9*(1), 62–66. https://doi.org/10.1109/TSMC.1979.4310076

Parrish, C. E., Magruder, L., Herzfeld, U., Thomas, N., Markel, J., Jasinski, M., et al. (2022). ICESat-2 bathymetry: Advances in methods and science. In *OCEANS 2022, Hampton roads* (pp. 1–6). https://doi.org/10.1109/OCEANS47191.2022.9977206

Parrish, C. E., Magruder, L. A., Neuenschwander, A. L., Forfinski-Sarkozi, N., Alonzo, M., & Jasinski, M. (2019). Validation of ICESat-2 ATLAS bathymetry and analysis of aTLAS's bathymetric mapping performance. *Remote Sensing*, *11*(14), 1634. https://doi.org/10.3390/rs11141634

Peng, K., Xie, H., Xu, Q., Huang, P., & Liu, Z. (2022). A physics-assisted convolutional neural network for bathymetric mapping using ICESat-2 and Sentinel-2 data. *IEEE Transactions on Geoscience and Remote Sensing*, *60*, 1–13. https://doi.org/10.1109/TGRS.2022.3213248

Shangguan, M., Liao, Z., Guo, Y., & Lee, Z. (2025). Seabed backscattered signal peak shift and broadening induced by multiple scattering in bathymetric lidar. *IEEE Transactions on Geoscience and Remote Sensing*, *63*, 1–14. https://doi.org/10.1109/TGRS.2025.3538989

Sokolova, M., & Lapalme, G. (2009). A systematic analysis of performance measures for classification tasks. *Information Processing and Management*, *45*(4), 427–437. https://doi.org/10.1016/j.ipm.2009.03.002

Stumpf, R. P., Holderied, K., & Sinclair, M. (2003). Determination of water depth with high-resolution satellite imagery over variable bottom types. *Limnology & Oceanography*, *48*(1part2), 547–556. https://doi.org/10.4319/lo.2003.48.1_part_2.0547

Teh, H., & Hashim, A. (2014). Submerged modular breakwaters for coastal protection. *Advances in Fluid Mechanics*, *82*, 121–130.

Telem, G., & Filin, S. (2013). Photogrammetric modeling of the relative orientation in underwater environments. *ISPRS Journal of Photogrammetry and Remote Sensing*, *86*, 150–156. https://doi.org/10.1016/j.isprsjprs.2013.10.001

Thomas, N., Pertiwi, A. P., Traganos, D., Lagomasino, D., Poursanidis, D., Moreno, S., & Fatoyinbo, L. (2021). Space-borne cloud-native satellite-derived bathymetry (SDB) models using ICESat-2 and Sentinel-2. *Geophysical Research Letters*, *48*(6), e2020GL092170. https://doi.org/10.1029/2020GL092170

Wang, N., Gao, Y., Guo, H., & Lu, J. (2023). Analysis of characteristics of Tide and tidal current in the east China seas. *Journal of Physics: Conference Series*, *2486*(1), 012039. https://doi.org/10.1088/1742-6596/2486/1/012039

Wang, Y., He, X., Bai, Y., Wang, D., Zhu, Q., Gong, F., et al. (2022). Satellite retrieval of benthic reflectance by combining lidar and passive high-resolution imagery: Case-i water. *Remote Sensing of Environment*, *272*, 112955. https://doi.org/10.1016/j.rse.2022.112955

Werdell, P. J., Franz, B. A., Bailey, S. W., Feldman, G. C., Boss, E., Brando, V. E., et al. (2013). Generalized ocean color inversion model for retrieving marine inherent optical properties. *Applied Optics*, *52*(10), 2019–2037. https://doi.org/10.1364/AO.52.002019

Xie, C., Chen, P., Pan, D., Zhong, C., & Zhang, Z. (2021). Improved filtering of ICESat-2 lidar data for nearshore bathymetry estimation using Sentinel-2 imagery. *Remote Sensing*, *13*(21), 4303. https://doi.org/10.3390/rs13214303

Yang, F., Jian, Z., Ning, Y., & Li, Z. (2023). System design and technical innovation of BJ-3A/B satellites. *Spacecraft Engineering*, *32*(3), 7–15. https://doi.org/10.3969/j.issn.1673-8748.2023.03.002

Yang, F., Lu, X., Li, J., Han, L., & Zheng, Z. (2011). Precise positioning of underwater static objects without sound speed profile. *Marine Geodesy*, *34*(2), 138–151. https://doi.org/10.1080/01490419.2010.518501

Yang, J., Ma, Y., Zheng, H., Gu, Y., Zhou, H., & Li, S. (2023). Analysis and correction of water forward-scattering-induced bathymetric bias for spaceborne photon-counting lidar. *Remote Sensing*, *15*(4), 931. https://doi.org/10.3390/rs15040931

Yuan, X., Guo, L., Luo, C., Zhou, X., & Yu, C. (2022). A survey of target detection and recognition methods in underwater turbid areas. *Applied Sciences*, *12*(10), 4898. https://doi.org/10.3390/app12104898

Zhang, G., Xing, S., Xu, Q., Guo, S., Li, P., & Wang, D. (2024). Performance of landsat ETM plus, OLI and OLI-2 imagery in ICESat-2-Aided coastal bathymetry: The effect of radiometric resolution. *IEEE Access*, *12*, 148645–148652. https://doi.org/10.1109/ACCESS.2024.3401626

Zhang, Z., Yang, N., & Yang, Y. (2024). Autonomous navigation and collision prediction of port channel based on computer vision and lidar. *Scientific Reports*, *14*(1), 11300. https://doi.org/10.1038/s41598-024-60327-9

Zheng, H., Liu, H., Yang, J., Ma, Y., & Hua Wang, X. (2025). Deriving water diffuse attenuation coefficient Kd using ICESat-2 bathymetric information. *IEEE Geoscience and Remote Sensing Letters*, *22*, 1–5. https://doi.org/10.1109/LGRS.2024.3494800

Zhuang, Q., Zhang, J., Cheng, L., Chen, H., Song, Y., Chen, S., et al. (2022). Framework for automatic coral reef extraction using Sentinel-2 image time series. *Marine Geodesy*, *45*(3), 195–231. https://doi.org/10.1080/01490419.2022.2051648

References From the Supporting Information

Huang, Y., Yang, H., Tang, S., Liu, Y., & Liu, Y. (2023). An appraisal of atmospheric correction and inversion algorithms for mapping high-resolution bathymetry over coral reef waters. *IEEE Transactions on Geoscience and Remote Sensing*, *61*, 1–11. https://doi.org/10.1109/TGRS.2023.3271632

Lee, Z., Shang, S., Hu, C., Du, K., Weidemann, A., Hou, W., et al. (2015). Secchi disk depth: A new theory and mechanistic model for underwater visibility. *Remote Sensing of Environment*, *169*, 139–149. https://doi.org/10.1016/j.rse.2015.08.002

Levy, R. C., Mattoo, S., Munchak, L. A., Remer, L. A., Sayer, A. M., Patadia, F., & Hsu, N. C. (2013). The collection 6 MODIS aerosol products over land and ocean. *Atmospheric Measurement Techniques*, *6*(11), 2989–3034. https://doi.org/10.5194/amt-6-2989-2013

Reichstetter, M., Fearns, P., Weeks, S., McKinna, L., Roelfsema, C., & Furnas, M. (2015). Bottom reflectance in ocean color satellite remote sensing for coral reef environments. *Remote Sensing*, *7*(12), 16756–16777. https://doi.org/10.3390/rs71215852

Spitzer, D., & Dirks, R. W. J. (1987). Bottom influence on the reflectance of the sea. *International Journal of Remote Sensing*, *8*(3), 279–308. https://doi.org/10.1080/01431168708948642

Wu, Z., Mao, Z., Shen, W., Yuan, D., Zhang, X., & Huang, H. (2022). Satellite-derived bathymetry based on machine learning models and an updated quasi-analytical algorithm approach. *Optics Express*, *30*(10), 16773–16793. https://doi.org/10.1364/OE.456094